A Plasma-Switch Impedance Tuner With Microsecond Reconfiguration

Justin Roessler, *Graduate Student Member, IEEE*, Alden Fisher, *Graduate Student Member, IEEE*, Austin Egbert, *Member, IEEE*, Zach Vander Missen, Trevor Van Hoosier, *Graduate Student Member, IEEE*, Charles Baylis, *Senior Member, IEEE*, Mohammad Abu Khater, *Senior Member, IEEE*, Dimitrios Peroulis, *Fellow, IEEE*, and Robert J. Marks, II, *Life Fellow, IEEE*

***Abstract*— With many frequency bands previously allocated solely for radar now being reallocated for sharing, radar transmitters must be frequency-agile, able to quickly change operating frequency while maintaining detection range. This article details the design of a 2–4-GHz reconfigurable impedance tuner using 35-W plasma switches. The tuner consists of switched shunt capacitor and inductor branches loading a series microstrip line. For many RF matching applications, a reconfigurable impedance tuner must have a broad tuning bandwidth, real-time switching speeds, high power handling, low loss, and broad Smith chart coverage. The implementation of the tuner using semiconductor plasma switches illuminated by laser diodes is described. The tuner is demonstrated in measurements using a custom search algorithm, adjusting and optimizing the tuner settings to provide maximum output power in approximately 300 μs upon changes in operating frequency or antenna impedance. This tuner provides superior reconfiguration times over other high-power tuners in the literature. The tuner possesses losses as low as 0.77 dB and at least 30% Smith chart coverage over the entire tunable bandwidth. With a 26.7-μs switching speed, the impedance tuner is also demonstrated to handle 20 W of power at all frequencies and states with over 40 W of power for greater than half of the octave bandwidth and power handling measured as high as 70 W. The combination of fast reconfiguration and high power handling in an impedance tuner can enable cognitive radar systems to adapt to a congested and dynamic environment in real time.**

***Index Terms*— Cognitive radar, diode lasers, electronic components, high-speed electronics, impedance matching, power semiconductor switches, tunable circuits and devices, tuners.**

Manuscript received 11 July 2022; revised 25 October 2022; accepted 31 October 2022. Date of publication 1 December 2022; date of current version 13 January 2023. This work was supported by the Office of Naval Research through the Department of Navy Award under Award N00014-19-1-2549. This article is an expanded version from the 2022 IEEE MTT-S International Microwave Symposium, Denver, Colorado, June 2022 [DOI: 10.1109/IMS37962.2022.9865404]. *(Corresponding author: Charles Baylis.)*

Justin Roessler, Austin Egbert, Trevor Van Hoosier, Charles Baylis, and Robert J. Marks, II, are with the Department of Wireless and Microwave Circuits & Systems (WMCS), Baylor University, Waco, TX 76706 USA (e-mail: justin_roessler@baylor.edu; austin_egbert@baylor.edu; trevor_vanhoosier1@baylor.edu; charles_baylis@baylor.edu; robert_marks@baylor.edu).

Alden Fisher, Zach Vander Missen, Mohammad Abu Khater, and Dimitrios Peroulis are with the School of Electrical and Computer Engineering, Purdue University, West Lafayette, IN 47907 USA (e-mail: fishe128@purdue.edu; zvanderm@purdue.edu; mabukhat@purdue.edu; dperouli@purdue.edu).

Color versions of one or more figures in this article are available at https://doi.org/10.1109/TMTT.2022.3223344.

Digital Object Identifier 10.1109/TMTT.2022.3223344

I. Introduction

IN THE increasingly congested and contested RF spectrum, there is a growing need for adaptive radar systems that can react to interference from other users while still maintaining optimal system performance. The 3.45-3.55-GHz subband, originally allocated to radar in USA, was reallocated for sharing, with fifth-generation (5G) wireless providers as the primary user [1] in August 2020. In October 2021, the Department of Defense and the National Spectrum Consortium launched the Partnering to Advance Trusted and Holistic Spectrum Solutions (PATHSS) to collaborate on exploring sharing solutions in the 3.1–3.45-GHz frequency range enabling these frequencies for commercial 5G use [2]. With this initiative, 5G applications would gain significant access to the 3.1–3.98-GHz frequency band. The *S*-band is being targeted for 5G use because it provides a good compromise between low propagation attenuation and high available bandwidth [3]. Since radar systems now need to share the *S*-band, their transmitters will require quickly reconfigurable, high-power handling impedance tuners capable of rematching the power amplifier (PA) upon changes in frequency or array scan angle to maximize output power and hence detection range, as shown in Fig. 1. The PA load reflection coefficient providing maximum output power changes with frequency, and the value of antenna reflection coefficient can change significantly with array scan angle [4]. Both situations require reconfiguration of the impedance tuner for maximum power transmission.

Prior work demonstrates that the use of a reconfigurable impedance tuner in a PA can provide a 16.7% improvement in radar range compared to a fixed broadband matching network [5]. This is an experimental manifestation of the Bode-Fano criteria, which express the tradeoff between gain and bandwidth [6], [7]. Yarman [8] further describes challenges with gain presented by broadband matching networks. Using a tunable matching network, the advantages of high gain achievable through a narrowband design can be achieved because the narrowband match can be moved through reconfiguration to be centered at the desired operating frequency.

The literature contains demonstrations of impedance tuner designs capable of either fast reconfiguration or high power handling. However, in most cases, both characteristics are not simultaneously realized. Ferroelectric tuners provide

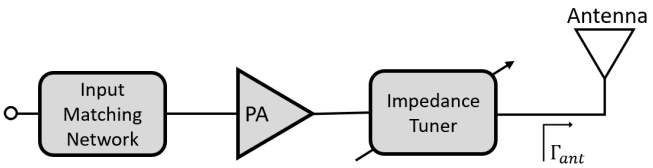

Fig. 1. Illustration of placement of impedance tuner in PA. Reprinted from [24].

microsecond adaptability but are typically limited to about 1 W of power handling [9], [10]. Because they rely on the physical movement of components, mechanical resonant-cavity tuners, while able to handle high power, typically require from milliseconds to seconds to reconfigure [11]. Commercial slide-screw impedance tuners used for laboratory device characterization typically take even longer to reconfigure [12]. Varactor tuners [13], electrically actuated through a change in bias voltage, are capable of fast reconfiguration but perform nonlinearly at relatively low power levels. Tuners demonstrating reconfiguration in tens of microseconds can often only handle single-digit watt power levels [14], [15]. For radar applications, a tuner with sub-millisecond reconfiguration time and power handling in the tens of watts is desired.

In addition to the physical aspects of the tuner enabling fast reconfiguration, efficient search algorithms must be designed to allow measurement-based decisions for quickly optimizing the tuner performance "on the fly" with as few measurements as possible. Algorithms for controlling various impedance tuners are shown in [16], [17], and [18] using directed, genetic, and exhaustive searches. With an algorithm for controlling an impedance tuner, the device can be integrated into a full system. Dockendorf et al. [19] demonstrated control of a mechanical evanescent-mode cavity tuner designed by Semnani et al. [11] using a software-defined radio (SDR) platform. While useful, the system is limited by the slow tuner reconfiguration time, which causes the system to spend a significant amount of time operating at a nonoptimal state. Because cognitive, spectrum-sharing radars must change frequencies quickly to avoid interference, the optimal state of the tuner is typically changing at a rate that is orders of magnitude faster than the tuner's reconfiguration time. One solution to this problem is to optimize the tuner for average performance, as demonstrated in [20]. In this implementation of the Semnani tuner, an asynchronous gradient optimization of average performance is used to overcome slow tuning time. This implementation allows the radar to operate continuously without having to wait long periods of time for an optimization to complete. However, since the optimization only looks at average power over several different waveforms, the actual maximum output power is not obtained. A fast impedance tuner is needed to fully maximize the radar range on a pulse-to-pulse basis for many radars. An electrically actuated tuner with high power handling is needed to accomplish these objectives.

Calabrese et al. [22] demonstrated an initial switched-stub tuner design with low-power field-effect transistor (FET) switches [21] and high-power switches constructed from semiconductor plasma. The stub tuner uses radial stubs connected to a series feedline through switches. The plasma switches are demonstrated by Fisher et al. [23] to handle up to 35 W of continuous-wave (CW) power. While the switched-stub tuner can perform a reconfiguration optimization within microseconds under the control of an SDR, the significant loss was observed at many of the tuning states [22]. For the high-loss states, the disadvantage of the loss outweighs the benefit of improved matching. In this article, a tuner with improved loss performance is demonstrated with switched shunt capacitor networks and shunt inductor networks. The tuner provides broad Smith chart coverage and low loss over the 2-4-GHz octave, fast optimization capability, and high power handling.

This article is an extension of [24] that presents the topology of the tuner and shows a fast optimization algorithm, along with assessment of Smith chart coverage and loss. This present article extends these results by describing a formalized approach by which switched-stub tuners can be generally designed to meet a set of tuner specifications and by assessing full power-handling limitations of the tuner in theory and in measurement. As such, the main contributions of our work include the combination of fast tuning and high power handling in the reconfigurable impedance tuner, and a method for specification-based design and power-handling assessment of a tuner.

II. Switched-Network Impedance Tuner Design

Several efforts to design impedance tuners with switchable networks exist in the literature. Vai and Prasad [25] discussed real-time impedance matching using tuning stubs with adjustable microstrip techniques for both hybrid circuits and monolithic microwave integrated circuits (MMICs). Unlu et al. [26] presented an impedance matching circuit using three stubs of variable length, which make use of distributed MEMS transmission lines. While MEMS can be used very effectively for fast reconfigurability, however, its power handling and linearity are limited. Yokota et al. [27] presented a method using liquid stub tuners for real-time impedance matching in ion cyclotron range of frequencies (ICRF) heating, but complete reconfiguration can take as long as 40 s. The design by Calabrese, using plasma switches with variable-length open-circuit stubs, appears to present good power handling and fast switching time, but the stubs result in a significant loss at many tuning states [22].

An impedance tuner with switched shunt networks is designed by presenting N branches of shunt inductors or capacitors spaced along a 50-Ω main transmission line (feedline). The shunt inductors and capacitors, with the transmission-line segments that connect them, and additional parasitic resistances and other effects present 2^N combinations of impedance points able to be reached on the Smith chart.

Each state has an N-bit binary representation, where each bit represents one of the switches, with an "ON" switch represented by 1 and an "OFF" switch represented by 0. An example of one of the 2^N states, State 001100 (binary) = 12 (decimal), is shown in Fig. 2 with its matching from a 50-Ω load shown in Fig. 3. In this state, the middle two switched shunt networks are switched ON, while the other switches

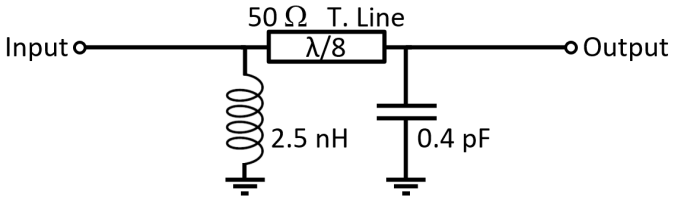

Fig. 2. Illustration of state 12 of the plasma-switched impedance tuner.

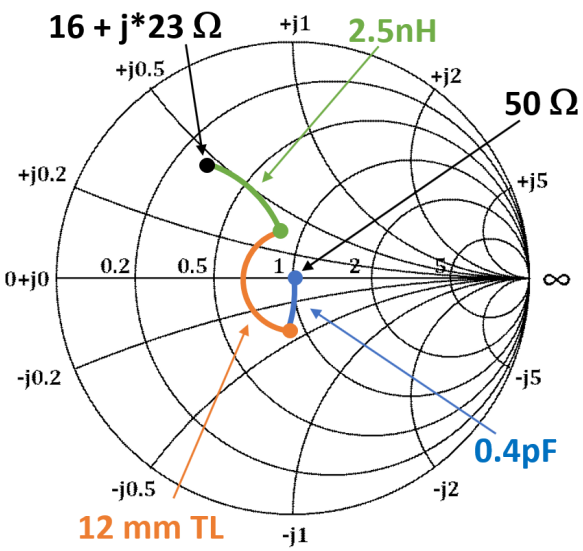

Fig. 3. Illustration of the plasma-switched impedance tuner state 12 rotation on Smith chart assuming 50-Ω and ideal components at 3 GHz.

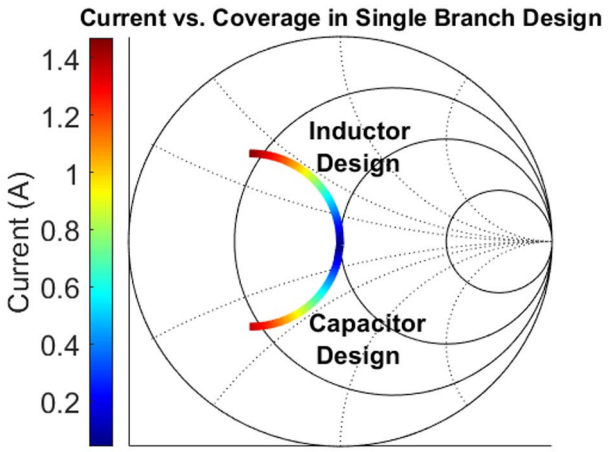

Fig. 4. Smith chart coverage versus current for a single branch inductor (top arc) and capacitor (bottom arc) component value sweep.

are OFF. On the output side, 50 Ω is presented, as it consists of the 50-Ω feedline terminated in the 50-Ω load presented by the next stage. If an inductor and capacitor are used, respectively, for shunt networks 3 and 4 (the networks switched "ON"), the equivalent circuit appears as in Fig. 2.

Fig. 3 shows the trajectory traversed on the Smith chart at 3 GHz for a 2.5-nH inductor and a 0.4-pF capacitor spaced apart by an 80° electrical length 50-Ω transmission line. In the pictured case, the impedance presented to the output of the PA is shifted from 50 Ω to $(16 + j23)$ Ω. From this simple illustration, the ability to provide Smith chart coverage is visualized. Capacitors provide downward movement on the chart, whereas inductors provide upward motion. The emanating point for each component's motion is based on the transmission-line lengths between the components.

Through choices of different capacitor and inductor values for the switched states of the tuner, different regions of the Smith chart can be presented to the amplifier. However, power handling and loss for these different shunt networks must also be analyzed, in addition to the Smith chart coverage they provide. The coverage of a switched impedance tuner depends on the level of susceptance in each branch presented by the shunt capacitor or inductor it contains. While high susceptances allow coverage closer to the edge of the Smith chart, high susceptances allow more current to be drawn into the branch, resulting in greater loss of the plasma switch, as well as greater resistive loss in the transmission-line elements and the parasitic resistance of the capacitor or inductor. As such, improved Smith chart coverage unfortunately results in greater loss. Furthermore, the increased current resulting from higher susceptance results in reaching the current limitation of the chiplet at a much lower input RF power, reducing the tuner's power handling in these states. As such, increased Smith chart coverage tends to be accompanied by increased loss and decreased power handling.

To assess the correlation of shunt-element current with matching capability, a simulation was performed using a constant 35-W input power to a tuner with a single shunt branch exposed through an "ON" switch (all other branches used "OFF" switches). The simulations were conducted with models for the plasma switch, transmission lines, inductor, and capacitor. Fig. 4 shows the location on the Smith chart of shunt elements of differing inductive and capacitive susceptance terminated in a $Z_0 = 50$ Ω load. A color map is placed on the trace indicating the root-mean-square (rms) current through the shunt inductor or capacitor, dependent on its value.

As the shunt element increases in susceptance magnitude, causing the trace to extend further toward the Smith chart edge, the current through the shunt branch is increased. In the semiconductor plasma chiplet switches used for this tuner design, the chiplets each possess a 0.82-A_{RMS} current limit specification, so greater coverage could lead to failure at a lower RF input power. Also, the increase in I^2R loss with increased current impacts the tuner loss of each state: greater susceptance in the shunt elements, while enhancing coverage, results in more loss.

Expanding on the single-branch switched tuner sweep, a two-branch switched tuner is developed for the four possible combinations of inductors and capacitors. In a simulation of these topologies, the inductor and capacitor values were swept to assess the impacts of coverage on the branch currents. Fig. 5 shows the coverage and average rms current (averaged over the two branches) for the four different possible topologies based on a choice of inductor or capacitor in each branch. Like a single-branch tuner, the average branch current increases with distance from the center of the Smith

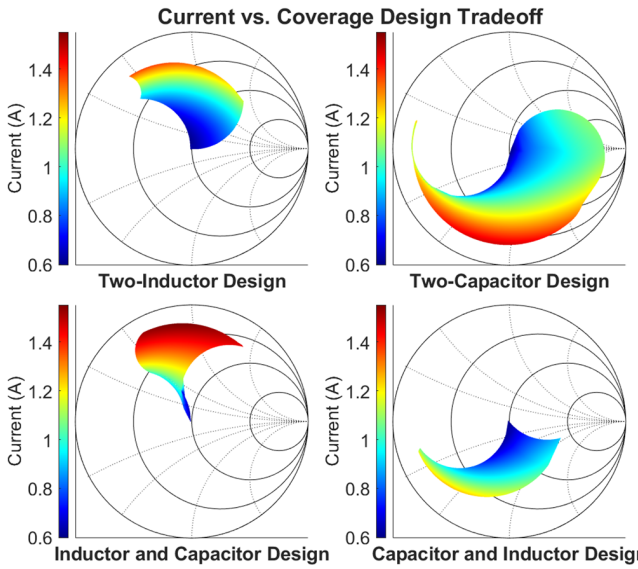

Fig. 5. Smith chart coverage versus average branch current for all combinations of a two-branch tuner using inductors and capacitors on the same color scale.

chart, causing higher loss and lower power handling based on current-handling limitations of the switches.

In considering how this tradeoff expands to an N-branch impedance tuner, it is evident that high inductive or capacitive susceptances, while providing greater coverage, result in increased branch currents, which are accompanied by increased loss and degraded tuner power handling. High susceptances should therefore be avoided. As such, multiple low-susceptance branches should be utilized in a tuner design to collectively maintain the reach of Smith chart coverage while also providing a denser coverage region (more states), lower tuner losses, and higher power handling than fewer high susceptance branches can achieve for a given Smith chart coverage.

With understanding of the tradeoff between coverage, loss, and power handling, a tuner design process using inductors and capacitors can be developed to design a switched-network impedance tuner design. The designer should strive to minimize tuner loss and maximize power handling (through minimizing branch currents) constrained by specifications on tunable bandwidth, percent Smith chart coverage, and the number of tunable impedance points required in a design. Fig. 6 shows the layout of a generalized initial tuner structure of this topology, and the flowchart of Fig. 7 depicts the process for designing a switched-network impedance tuner, given the required tunable bandwidth, percent Smith chart coverage, and desired number of impedance points. To meet tuner specifications with the best loss and power handling, the number of branches, sequence of inductors and capacitors, and the values of the inductors and capacitors can be selected to provide the best performance. The number of branches, specified as N, is calculated depending on the number of impedance points (Z_{count}) required in a design and is shown in (1). The number of branches can be increased if greater coverage is desired. The feedline width is calculated to have a 50-Ω characteristic

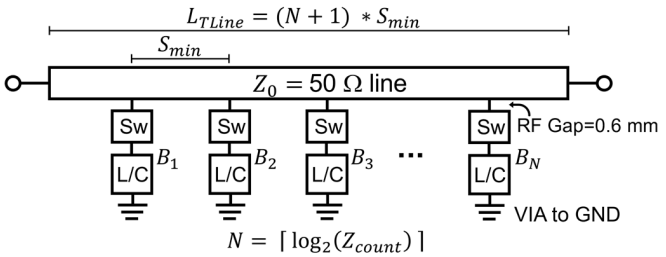

Fig. 6. Layout of the initial tuner structure. L_{TLine} is the total length of the transmission line, S_{min} is the minimum feasible branch spacing, B_n is the spacing between branches n and $n+1$, and N is the number of switched shunt networks, calculated based on the number of impedances Z_{count} to be provided by the tuner.

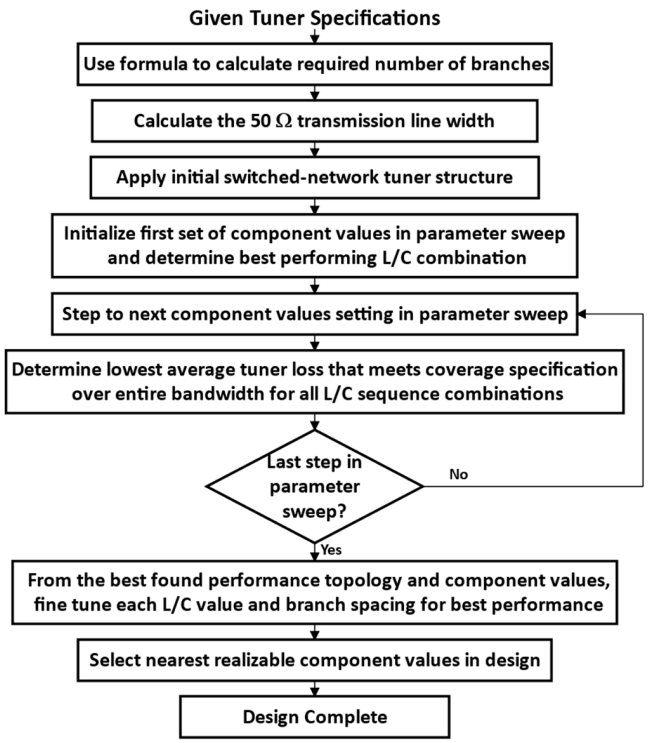

Fig. 7. Standardized switched-network impedance tuner design process given tuner specifications on required tunable bandwidth, percent Smith chart coverage, and number of impedance points required on the Smith chart.

impedance for minimal loss. The length of the feedline, L_{TLine}, is determined by the minimal feasible spacing between each switch, S_{min}, and the number of branches, N, required in a design and is shown in (2)

$$N = \lceil \log_2 (Z_{\text{count}}) \rceil \tag{1}$$

$$L_{\text{TLine}} = (N+1) * S_{\text{min}}. \tag{2}$$

The main impact branch spacing that has on the tuner design is the tuner loss for each state. Since loss increases with length in a physically realizable, lossy microstrip transmission line, the smallest feasible feedline is optimal. While tuning each of the branch spacings ($B_1, B_2, \ldots, B_N$) will rotate a portion of the impedance points about the center of the Smith chart to get a more uniform spread of impedance points,

tuning the branch spacings does not have a significant impact on the magnitude of the coverage reach or power-handling capabilities. Thus, the branch spacing is set to the smallest feasible spacing to meet the footprint requirements of the laser diodes until the final steps of the design process when the coverage can be fine-tuned to achieve a more uniform Smith chart coverage area, as shown in Fig. 7.

Based on the physical constraints of the laser diodes in the plasma switches [23], a minimum $S_{\min} = 10$ mm branch spacing is required to place the laser diodes in their proper position over each chiplet. Also, a 0.6-mm gap between the main transmission line and the start of a shunt branch was used to allow each switch to be placed between its branch and the feedline. The power handling of each plasma switch is limited by the chiplet's 0.82-A_{RMS} current handling. To model the switch for analysis, a 4-Ω ON-state resistance and a 60-fF OFF-state capacitance were used.

With the initial tuner structure in place, the topology and values of the capacitors and inductors are iteratively selected, stepping through all possible L/C sequences and a range of component values. The "best performance topology" in Fig. 7 is defined as the topology that provides the lowest average tuner loss over the bandwidth while providing the specified minimum Smith chart coverage. For the iterative parameter sweep, the capacitor values of 0.1, 0.2, 0.5, 1, and 2 pF and the inductor values of 1.5, 2.4, 4, 6.4, 10.5, and 17 nH were used. For each set of L/C values in the parameter sweep, all L/C combinations are analyzed to determine the best switched-network tuner topology performance given the set specifications. After determining the best tuner topology, fine-tuning of each of the branch spacings $B_1, B_2, \ldots, B_N$ is performed to try to achieve the uniform coverage area. The final step in the standardized process is the selection of purchasable component values. With this process, a switched-network impedance tuner can be developed to meet a wide variety of tuner design specifications.

Since low-admittance branches do not provide sufficient Smith chart coverage and high-admittance branches incur more loss in each state, providing impedance matching to increase output power is multifaceted. The goal to obtain an optimal switched-network tuner is to identify the optimal admittance region providing good Smith chart coverage with an acceptable low loss for each tuner state and to maintain this optimal admittance region over the entire tunable bandwidth of a design. However, both inductive admittance ($1/j\omega L$) and capacitive admittance ($j\omega C$) vary with frequency.

Over an octave bandwidth, capacitive admittance is doubled, whereas inductor admittance is halved. This allows a broad tunable bandwidth to be achieved in a switched tuner design. Using both inductors and capacitors, the optimal admittance region can be maintained over the entire tunable bandwidth. As frequency increases to the upper half of the tunable bandwidth, the inductor admittance becomes smaller and does not have much effect in changing the S-parameters of the tuner. Furthermore, as this transition occurs with inductors from good coverage to poor coverage, capacitors will transition opposite of the inductor. Thus, using both inductors and capacitors in switchable shunt networks can collectively maintain an admittance in the optimal admittance region over a broad bandwidth for balanced tuner performance. In the middle of the band, lower admittance branches of both inductors and capacitors can collectively be used to reach good coverage while incurring lower loss than the loss at the edges of the tunable band.

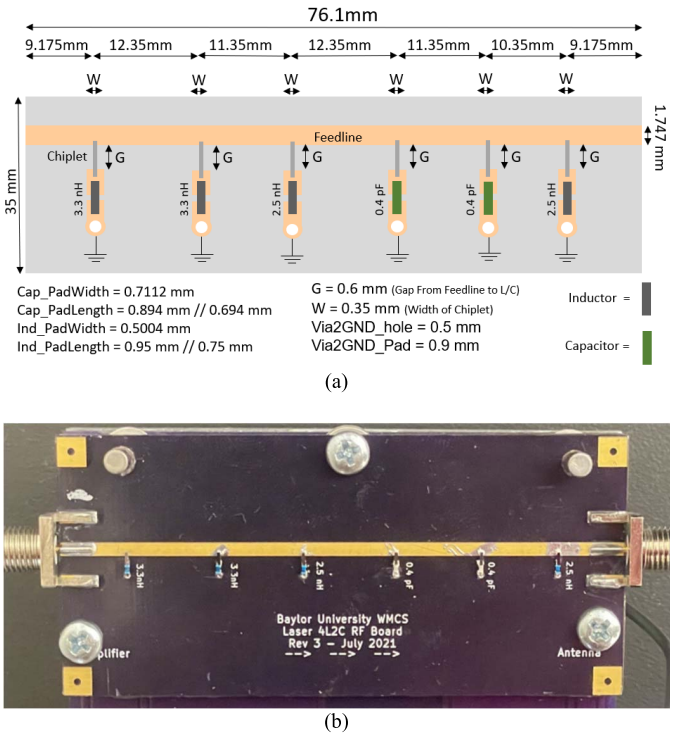

Fig. 8. (a) Plasma-switched impedance tuner design using grounded inductors and capacitors in a drawing (reprinted from [24]). (b) Fabricated RF board design containing the design.

After exhaustively stepping through all 2^N possible inductor and capacitor topology combinations for a variety of inductance and capacitance values, the optimal topology that best met the design goals was selected. With the best topology and component values for a high-power 6-bit digitally controlled tuner design determined, the optimal purchasable component values and spacings between each branch were set through the process of simulated parameter tuning and analysis. A drawing of the plasma-switched tuner design using inductors and capacitors terminated to the ground is shown in Fig. 8(a) [24] with the fabricated RF board holding the design shown in Fig. 8(b).

III. Simulation Results

The Momentum Microwave 2.5-D electromagnetic (EM) simulator in the Advanced Design System (ADS) software was used to model the EM properties of the tuner topology design and determine the optimal tuner design for our specifications. All physical components and interfaces were modeled in the design to ensure that accurate simulated tuner performance was maintained in the ADS model. Lumped-element components were represented with Modelithics passive component models in simulation. The finalized design uses four inductors

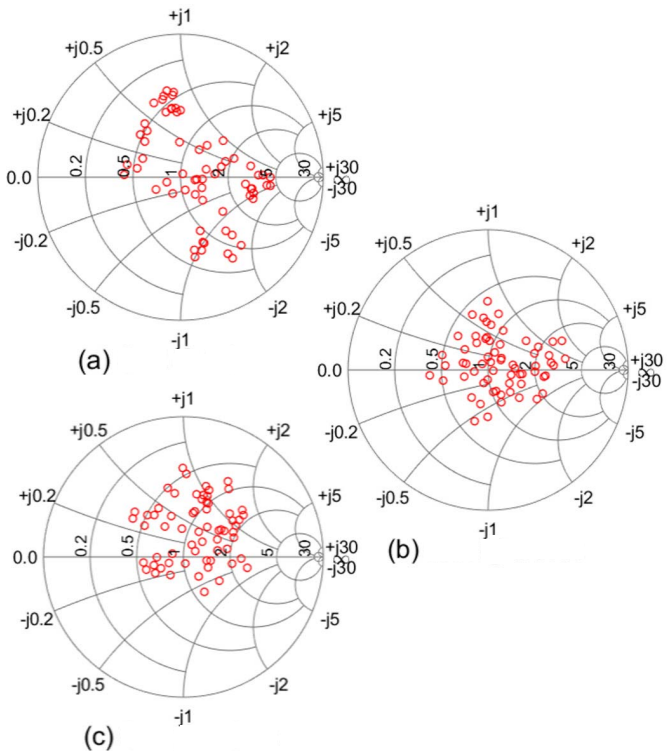

Fig. 9. Simulated Smith chart coverage of all 64 states at (a) 2, (b) 3, and (c) 4 GHz.

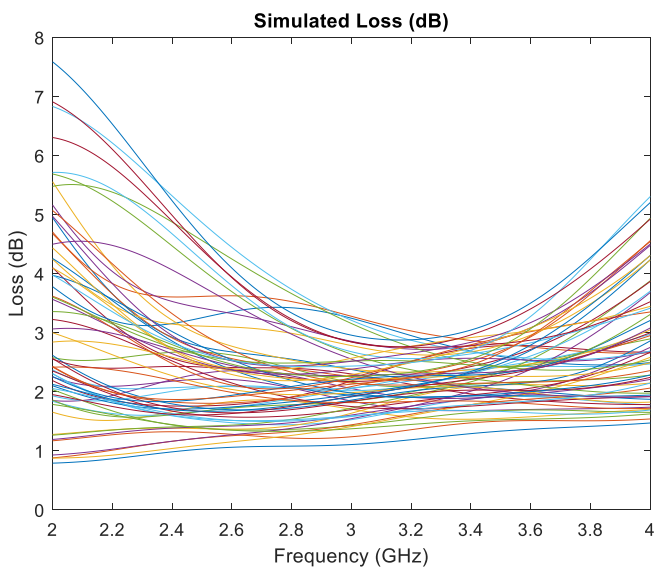

Fig. 10. Simulated loss of all 64 tuner states from 2 to 4 GHz.

and two capacitors in a 64-state digitally controlled impedance tuner. In the design, 3.3- and 2.5-nH inductors are used along with 0.4-pF capacitors. These components are placed in shunt to ground from the main feedline, resulting in six switched branches in the tunable matching network. Via models were used in ADS to model the connection through the board to the microstrip backside ground plane. The spacing between the components and the values of all components were optimized. The simulation results are shown in Figs. 9 and 10.

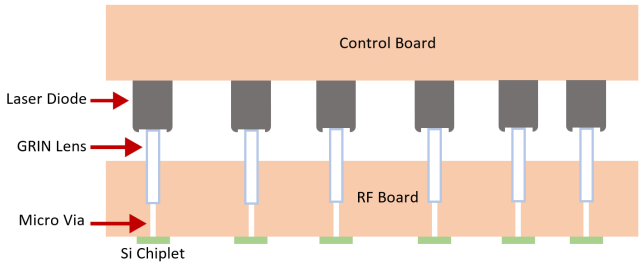

Fig. 11. Cross-sectional illustration of tuner alignment stack-up. Reprinted from [24].

Fig. 9 shows that the tuner coverage consistently provides approximately 30% coverage of the Smith chart over the 2–4-GHz band. As discussed in Section II, even greater Smith chart coverage can be obtained, but at the expense of greater loss. This design provides a good compromise between Smith chart coverage and reasonable loss performance. Fig. 10 shows that many of the states stay under 3 dB of loss in simulation over the entire 2–4-GHz tuning range. By utilizing inductors and capacitors instead of radial stubs, in-band quarter-wave resonances due to an open-circuit transmission line were no longer apparent in the design, which had caused very high currents to pass through the branches causing high loss and low power handling. Also, the inversely related transfer functions of the inductors and capacitors allowed more control to stay within the optimal admittance region for balanced performance over a broad bandwidth. States providing RF short circuits to the ground within the band were better avoided since radial stubs were not used. By improving the tuner design to reduce loss, the tuner will have more freedom and ability to improve output power through impedance matching.

IV. Impedance Tuner Fabrication

The fabricated tuner uses a two-board design, consisting of an RF board and a control board. The RF board has the design of Fig. 8(a), and the control board is used to set the state of the tuner and interfaces with a microcontroller or an SDR for executing the optimization algorithm. The RF board is a 31-mil FR4 board with 2-oz. copper microstrip traces and SMA connections. Fig. 11 shows the stack-up of the control board and RF board. The RF board includes nonplated through hole (NPTH) micro and blind vias. To focus the laser diode excitations, gradient index (GRIN) lenses were placed in the blind vias on the backside of the RF board. In each shunt branch, the chiplet spans across a 0.6-mm RF gap, and the vias are placed in the center of these gaps. The 0.15-mm micro-vias were drilled through the board to allow the laser excitation to pass onto the chiplet gap. A larger blind via (0.5 mm) was drilled concentrically, partially through the board, located at an ideal distance from the chiplet to focus the laser light at the chiplet gap. The use of the lenses and vias to focus the light is designed to reduce the insertion loss values of the plasma switches. The custom chiplets, developed by Fisher et al. [23], are 350 μm wide and 1.675 mm long to span the distance of the 600-μm RF gap. The chiplet's gap is 75 μm, which separates two gold sputtered regions, leaving

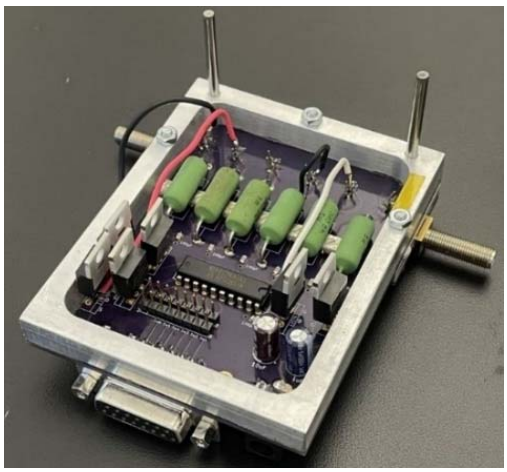

Fig. 12. Fabricated tuner design in isometric view.

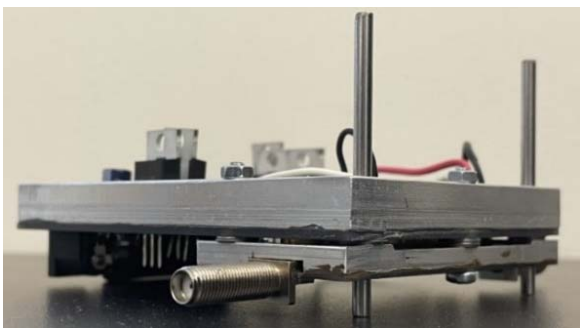

Fig. 13. Fabricated tuner design two-board alignment.

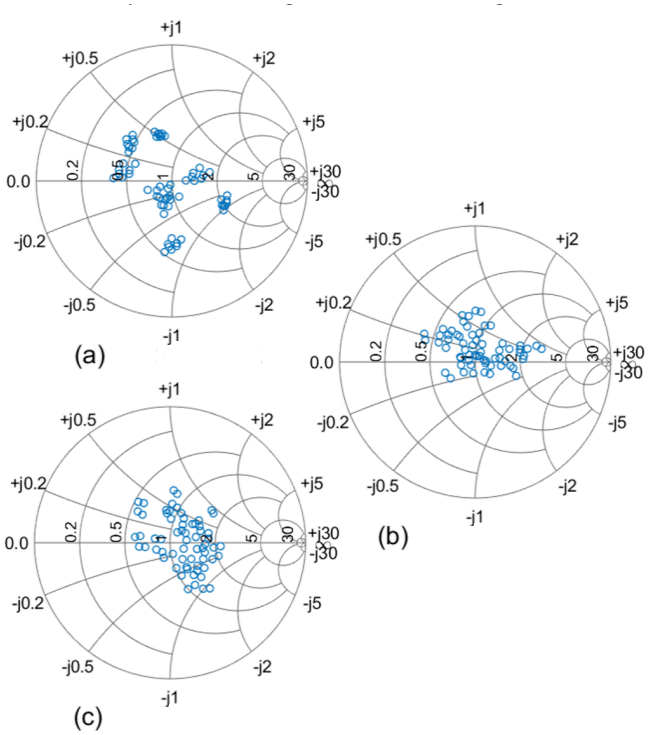

Fig. 14. Measured Smith chart coverage of all 64 states at (a) 2, (b) 3, and (c) 4 GHz. Reprinted from [24].

the switch disconnected when the plasma is not excited. When the plasma in the chiplet is excited by the 1-W 940-nm laser diodes, the switch is closed and the branch is connected to the feedline with its packaged inductor or capacitor, followed by a via to ground.

To maintain the minimal insertion loss of the semiconductor plasma switch, a repeatable and reliable alignment had to be implemented for the two-board tuner design. Figs. 12 and 13 show the fabricated tuner and the two-board alignment, respectively. High-precision alignment was found to be critical in obtaining repeatable results. Initial designs held the two boards in place by two plastic screws and nuts. However, when adjusting the screws, it was easy for the two boards to fall out of alignment since they require precision on the order of micrometers. A more sophisticated alignment method was implemented using precise custom machined aluminum brackets adhered to each board with steel screws and rods to firmly secure the boards in the optimal alignment between the lasers and the silicon chiplets. In this position, the laser diode junctions are precisely placed directly over the corresponding blind via. This maximizes the transfer of near-infrared laser light from the diode through the GRIN lens to the 75-μm chiplet gap, obtaining the optimal efficiency for plasma generation. This repeatable alignment enables lower loss and thus better matching performance.

V. Tuner Performance Measurements

The performance of the tuner was validated using measurements, in which an SDR and microcontroller were used to set the tuner state and implement the search algorithm. A Skyworks SKY65017-70LF amplifier with a 3-dBm input power was used as the amplifier device and a Maury Microwave Commercial load—pull tuner was used to emulate a changing antenna reflection coefficient Γ_{ant}. S-parameters of the tuner were measured using a vector network analyzer for performing loss and Smith chart coverage calculations. Fig. 14 shows the measured Smith chart coverage at 2, 3, and 4 GHz. The coverage range is maintained consistently across frequency and achieves 30% Smith chart coverage over the tunable bandwidth by estimating the percent coverage from the coverage plots. Tuner loss of each tuner state is defined by the following equation:

$$\text{Loss} = -10 * \log_{10}\left(\frac{|S_{21}|^2}{1-|S_{11}|^2}\right) = P_{\text{del,IN,dB}} - P_{\text{OUT,dB}} \quad (3)$$

which describes loss as the ratio between the power delivered to the input of the tuner and the tuner output power. This loss, therefore, does not include return loss. Loss for the plasma-switched tuner is plotted in Fig. 15 for all the 64 tuning states over the 2-4-GHz range.

As shown in Fig. 15, the impedance tuner design demonstrates tuner loss as low as 0.77 dB and an average tuner loss of only 2.5 dB. This is significantly improved from the predecessor to this design, shown in [22], which ranged up to 34 dB of loss. This lower loss means that numerous matching options are viable to improve output power, resulting in more consistent high-range radar detection capability. As described in [24], the 90%-10% on and off times were measured as 3.6 and 26.7 μs, respectively. These switching speeds will allow microsecond reconfiguration times in real time on

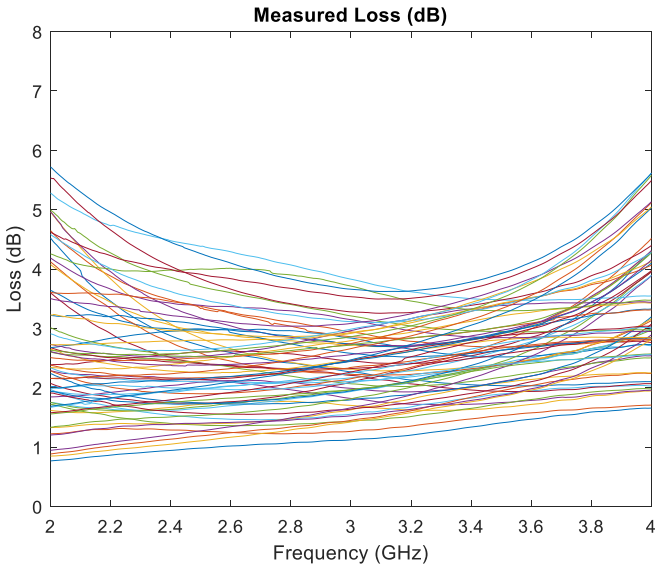

Fig. 15. Measured loss of all 64 tuner states from 2 to 4 GHz. Reprinted from [24].

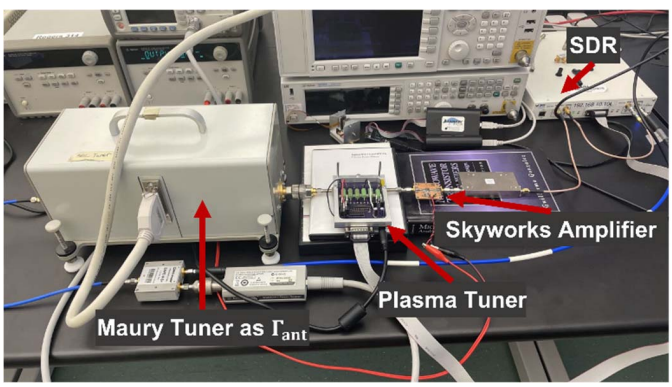

Fig. 16. Algorithm testing measurement setup.

a cognitive radar or in any other reconfigurable RF matching scenarios.

As described in [24], the fast optimization algorithm of [21] was applied to this tuner design. Measurement testing was performed using the Skyworks amplifier with 3-dBm input power and the Maury Microwave load—pull tuner to emulate the changing value of Γ_{ant}. The measurement setup is shown in Fig. 16 [24]. To test the algorithm, fast optimizations were performed from an SDR controller, with the results shown in Table I (reprinted from [24]). In the algorithmic search, the output power is evaluated with all switches OFF, and then, the switches are turned on one at a time, moving from input to output. If changing a switch disposition improves the output power, the switch is left in its new position. The search continues until a complete pass of all switches is performed with no improvement.

Table I shows the results of multiple searches performed at different combinations of operating frequency and antenna reflection coefficient (Γ_{ant}), including initial and final tuner output power values. The average search time is approximately 300 μs, and each individual search step required an estimated

TABLE I
TUNER OPTIMIZATION RESULTS [24]

Freq. (GHz)	Γ_{ant}	# Meas.	Time (µs)	Initial Power (dBm)	Best Power (dBm)	Best State [Bin (Dec)]
2.0	0.50/45°	10	297.79	11.73	14.32	010100 (20)
2.0	0.30/120°	10	297.79	12.29	14.34	011100 (28)
2.5	0	9	268.01	13.81	14.03	011000 (24)
2.5	0.30/120°	17	506.25	11.57	14.14	000011 (3)
3.0	0	12	357.35	12.02	12.20	000001 (1)
3.0	0.50/45°	10	297.79	6.55	10.21	000100 (4)
3.5	0.30/120°	12	357.35	6.45	8.53	000101 (5)
3.5	0.40/310°	12	357.35	5.72	8.49	010001 (17)
4.0	0	7	208.46	11.08	11.08	000000 (0)
4.0	0.32/10°	12	357.35	9.55	10.52	001001 (9)

maximum less than 27 μs. Because many of the states provide relatively low loss, a large variety of states can be seen as the "Best State" across these searches. Part of the decrease in maximum output power with increasing frequency is expected, due to the decrease of the Skyworks amplifier's maximum gain with increasing frequency. In addition, the limitations of Smith chart matching coverage can cause additional lowering of the maximum attainable output power. For example, in the 3.5-GHz test scenarios, the further drop in output power is caused by the optimal impedance matching being located near the edge of the Smith chart. Finally, it should be noted that the reference plane used for the output power assessment is at the tuner output. Overall, this tuner provides excellent versatility in achieving an acceptable match without large loss, providing superior reoptimization times over other high-power tuners. The accuracy of the match that can be provided, in addition to the tuner loss, combines to determine the output power.

VI. TUNER POWER-HANDLING MEASUREMENTS

The plasma-switched impedance tuner design has been demonstrated to have broad bandwidth, good coverage, low loss, and the ability to reconfigure in real time. The final requirement needed in an impedance tuner to be implemented in cognitive radar is high power handling. The power handling of the plasma-switched impedance tuner was assessed by further developing the Momentum Microwave 2.5-D EM tuner model to accurately predict the rms currents and voltages throughout the tuner given an input power, input impedance, and output impedance presented to the tuner, and then verifying the model with high-power measurement results. The tuner model can accurately predict the current levels through the switches by using an equivalent parallel *RC* circuit with an ON-state resistance and an OFF-state capacitance modeling the loss and isolation behaviors of the switch, respectively. In addition to the switch model, the models of the tuning inductors and capacitors, as well as the inductive vias to ground, are simulated allowing accurate prediction of the susceptance in each tuner branch. The susceptance levels in each branch for each state provide the simulator with enough information to determine the predicted current levels across the switches. Thus, from the predicted currents, the overall power handling

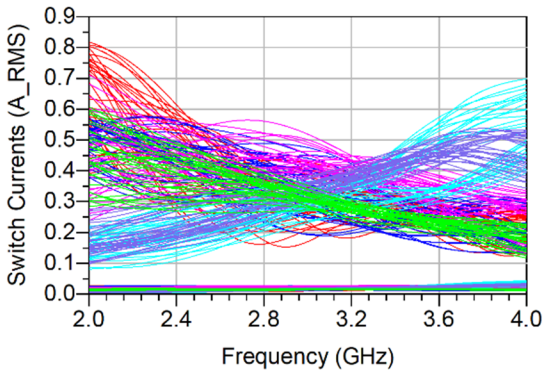

Fig. 17. High-power impedance tuner model current response for a 20-W input power and 50-Ω tuner source and load impedance.

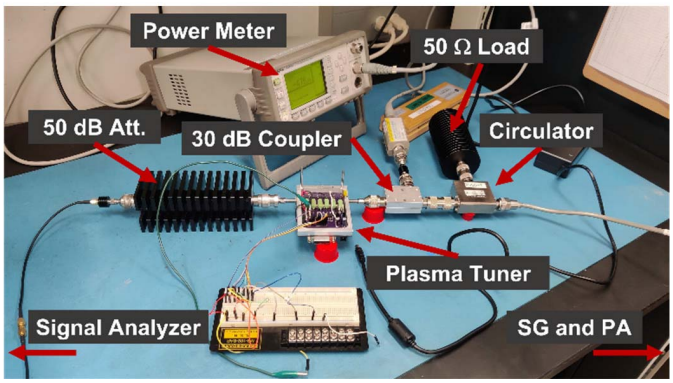

Fig. 18. High-power measurement setup.

of the tuner can be determined for numerous scenarios using the estimated switch electromigration failure current limit of 0.82 A_{RMS}. The tuner model is used to predict the input power level at which electromigration-related current failure will occur. In electromigration failure, atoms will undesirably move across the 75-μm chiplet gap, causing the switch to stick in short-circuit mode. To discern the RF power level at which failure is expected to occur, the current through all six switches over the 2–4-GHz frequency range is simulated, and the RF power is adjusted until the maximum current through any one of the switches in any of the tuner states is 0.82 A_{RMS}. Fig. 17 shows the model-predicted current through each switch in the tuner for a 20-W input power across all frequencies and tuner states. A maximum current of 0.82 A_{RMS} is observed at 2 GHz for the state with all switches ON (111111, state 63) when providing a 20-W input power. Providing any higher power level to the input of the tuner will cause higher branch currents to be observed, thus exceeding the current limit for the switch in state 63. Thus, this indicates that the RF power handling of the tuner is expected to be at least 20 W for all frequencies and states.

Interestingly, the high current states in the tuner occur at the ends of the octave tuning bandwidth. As discussed with the coverage versus loss tradeoff in Section II at 2 GHz, the inductor states present their highest susceptance, causing the most significant current to flow across the switches and then to ground. Likewise at 4 GHz, the capacitors states present their highest susceptance causing the most significant current to flow across the switches and then to ground. This relationship with current and loss versus coverage causes the limiting power handling of the tuner to occur at the ends of the band.

With a well-developed model, a series of measurements was performed to verify the model accuracy. The high-power measurement validation setup is shown in Fig. 18. The setup consists of a signal generator, amplifier, circulator, coupler, tuner, 50-dB load, and a signal analyzer. The signal generator and amplifier were selected to be able to deliver high power to the input of the tuner. A coupler was used in the measurement chain to verify the exact power that is available to the tuner as the measurement is performed. The signal analyzer was used to monitor the performance of the states and to observe failure when it occurs. Finally, the circulator and the 50-dB attenuator

TABLE II
HIGH-POWER MEASUREMENT RESULTS

Test	State	Freq.	Z_{ant}	Model Expected Failure	Measured Failure Power
1	16	4 GHz	110 – j45Ω	32 W	31.6-36.8 W
2	5	2 GHz	50 Ω	28 W	25 W
3	16	2 GHz	50 Ω	100+ W	70+ W

are used in the setup to protect the PA from reflected power. The input power to the tuner was increased in 5-W increments, starting at 10 W, until failure. The RF power was transmitted through the tuner for several seconds to establish successful operation at each power level tested.

The assembled test bench was used to perform three different tests to verify the accuracy of the tuner model. The Z_{ant} value of $*$ the first test required a non-50-Ω output impedance to the tuner and state 16 at 4 GHz. A good conjugate match and high current state were attainable for this scenario. This is a capacitor state, so it also was a higher current state to allow for easier failure within the framework of the test bench. The second and third tests resulted in 50-Ω output impedance to the tuner at 2 GHz for two different states. The states tested were states 5 and 16. The purpose of these tests was to measure a low current state (state 16 at 2 GHz) and a multiswitch ON state (state 5 at 2 GHz). The results of these measurement tests are outlined in Table II.

The failure powers of the three tests match closely with the expected failure power in the model. Test 3 shows how a low current state can reach much higher power levels before failure. The high power handling for this state is representative of other low current states in the tuner. In Test 3, the tuner successfully operated up to 70 W without failure. However, when ramping up the input power to the tuner beyond 70 W, dielectric air breakdown occurred causing the board to spark when no plasma switches ON. Thus, the measurement was stopped, and Table II reports the highest successful input power. Overall, the tests show that the 2.5-D EM plasma-switched tuner model accurately predicts the power handling of the impedance tuner design, especially at lower power handling states where electromigration failure occurs. The lower

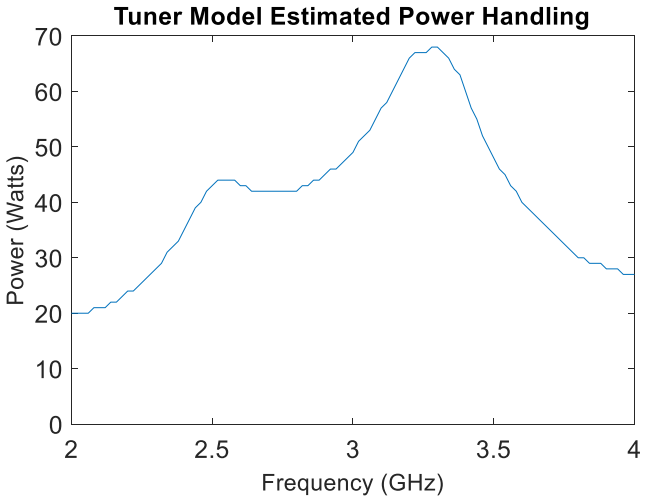

Fig. 19. Model estimated input power handling of the tuner from 2 to 4 GHz given a 0.82-A_{RMS} current limit for the chiplets.

bound of power handling is the main interest in this investigation since the tuner power handling is defined as the highest power level that all states can operate without failure in any given scenario. With confidence in the accuracy of the model, we can draw overall power handling conclusions on the tuner over frequency and Smith chart position.

The power handling of the tuner was estimated over frequency and then impedance position. After first conducting several simulations and sweeping input power to the tuner model, MATLAB postprocessing was used to determine the estimated power handling at each 10-MHz frequency step over the entire octave bandwidth of the tuner. Fig. 19 shows the estimated power handling of the tuner given a 0.82-A_{RMS} current limit for the chiplets since this estimate successfully predicted the approximate power of tuner failure in the previously described measurements. Given the current limit for the chiplets, lower susceptances of branches provide higher power handling, albeit at the expense of reduced Smith chart coverage.

Based on this analysis, Fig. 19 shows that the tuner can handle up to 68 W at 3.3 GHz. Furthermore, the tuner is shown to handle greater than 40 W over a bandwidth greater than half an octave. As described previously, the ends of the octave tuning bandwidth possess the lowest estimated power handling due to the tradeoff in the tuner design, showing power handling from 20 to 30 W at these frequencies. Overall, the tuner can handle at least 20 W of input power over the entire frequency band and over a 40-W power handling ability for greater than a half-octave of bandwidth in the tuner design.

Fig. 20 shows the power handling values for each of the attainable impedances from 2, 3, and 4 GHz on the Smith chart. In general, the power handling of the tuner can vary greatly from state to state with the best power handling impedance points near the center of the Smith chart. If desired, knowledge of the power handling capabilities of the tuner at different impedance combination points can be utilized to avoid matching at high current states. This would further improve the power handling of the tuner, as many impedance

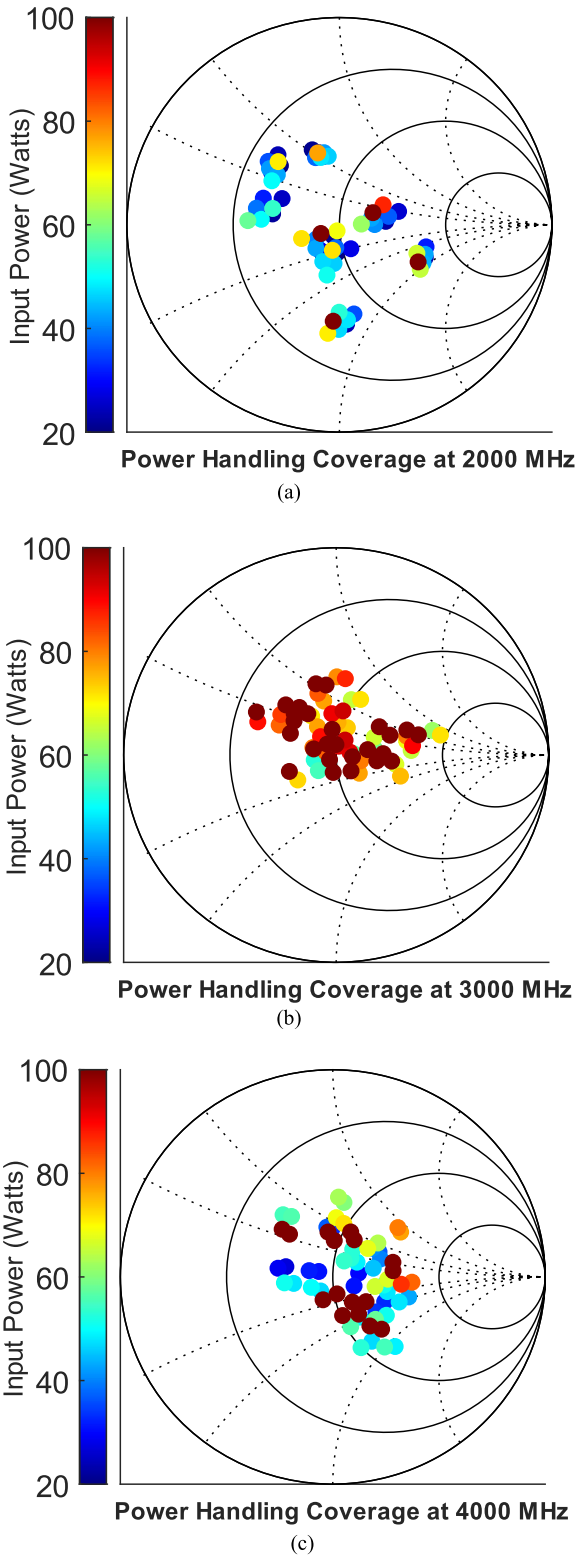

Fig. 20. Smith chart coverage power handling contour plot from the simulation model on the same color scale in watts at (a) 2, (b) 3, and (c) 4 GHz.

points achieve greater than 50-W power handling at each frequency of interest.

Table III compares the demonstrated plasma-switched impedance tuner to other state-of-the-art tuners in the literature. While a numerical comparison has been provided,

TABLE III
IMPEDANCE TUNER COMPARISON

Reference	Tuning Technology	Frequency (GHz)	Power Handling	Switch Time	Loss	Coverage$^{\uparrow}$
[9-10]	BST Capacitors	1.5 GHz – 2.0 GHz	0.63 W	< 5μs	2.5 dB – 6.5 dB	50 %
[14]	4 MEMS Varactors	27 GHz – 30 GHz	4 W	-	>3 dB	40 %
[15]	4 MEMS Varactors	1.0 GHz – 8.0 GHz	-	-	2.9dB – 4.6 dB*	75 %*
[13]	Varactors	2.0 GHz – 2.5 GHz	25 W	-	1 dB – 3 dB	55 %
[12]	Mechanical	0.4 GHz – 8.0 GHz	250 W	550 ms†	0.3 dB	>95 %
[11]	Linear Actuator	2.7 GHz – 4.4 GHz	100 W	9.22 ms^	0.56 dB	90 %
This Work	Plasma-Switched	2.0 GHz – 4.0 GHz	20 W	26.7 μs	0.77 dB – 5.7 dB	30 %
This Work	Plasma-Switched	2.84 GHz – 3.56 GHz	43 W	26.7 μs	1.08 dB – 4.03 dB	30%

†Per 10° at 2 GHz ^Per 10% actuator travel *Reported at 6 GHz $^{\uparrow}$Estimated from coverage plots and not directly reported

it should be kept in mind that the tuner of this present article was designed for an octave tuning bandwidth, significantly greater than many of the tuners in the comparison table. The plasma-switched tuner possesses an entire octave tuning bandwidth and high power handling of at least 20 W while providing superior reconfiguration speed over other high-power tuners. In addition, good Smith chart coverage and low tuner loss are maintained over an octave of tunable bandwidth. This tuner provides significant advancements in meeting the requirements needed for an impedance tuner design. Furthermore, over the same size fractional bandwidth as the Perez varactor tuner [13], the advantage in power handling in the plasma-switched impedance tuner becomes clear. The last line of Table III shows this: over the 2.84-3.56-GHz subband, the performance in switching speed, loss, and coverage is maintained, while power handling of the tuner increases to 43 W over all states and frequencies, nearly twice the power handling of the tuner in [13]. Additional improvements may have been obtained if the tuner were designed for this same operating bandwidth. Further improvement in Smith chart coverage would also be expected if our plasma-switched tuner design was developed for the same 2.84–3.56-GHz subband since the required tunable bandwidth would be much smaller. Table III shows advantages in tunable bandwidth, power handling, and switching speed while providing good loss and coverage. This real-time high-power impedance tuner will be a vital component in a cognitive radar system allowing maximum out power to be obtained with pulse-to-pulse reconfiguration, which provides the radar the freedom to quickly shift its operating frequency without the degradation of detection range.

VII. CONCLUSION

An *S*-band plasma-switched impedance tuner, with an octave tuning bandwidth, has been demonstrated to have good Smith chart coverage, low loss, real-time switching speeds, and high power handling for real-time RF matching applications. The tuner demonstrates 30% Smith chart coverage and only a 2.5-dB average tuner loss while maintaining a fast 26.7-μs switching speed and 20-W power handling over all frequencies and states. Furthermore, the power handling of the tuner is shown to have over 40-W capabilities for more than half of the octave tuning range, and power handling measured as high as 70 W. With the tuner demonstrating the ability to completely search and reoptimize in about 300 μs, on average, this provides superior reconfiguration times along with high power handling over a broad tunable bandwidth in a single tuner design. An approach for designing a switched-network impedance tuner has been provided and can be utilized in expanding this design approach to meet other tuner specifications. This tuner technology and design approach will enable radar systems to change frequencies and reoptimize performance on a pulse-to-pulse basis in many cases while providing frequency agility and maintaining maximum detection range.

ACKNOWLEDGMENT

The authors are grateful to Keysight Technologies for donation of the Advanced Design System software to Baylor University. They express appreciation to Modelithics for donation of model libraries to Baylor University through the Modelithics University Program. The United States Government has a royalty-free license throughout the world in all copyrightable material contained herein.

REFERENCES

[1] *White House and DOD Announce Additional Mid-Band Spectrum Available for 5G by the End of the Summer*, United States Dept. Defense, Washington, DC, USA, Aug. 2020.

[2] A. Keeney. (Oct. 27, 2021). National spectrum consortium launches PATHSS task group to explore 5G spectrum sharing. Business Wire. Accessed: Apr. 26, 2022. [Online], Available: https://www.businesswire.com/news/home/20211027005267/en/National-Spectrum-Consortium-Launches-PATHSS-Task-Group-to-Explore-5G-Spectrum-Sharing

[3] J. Horwitz. (Aug. 10, 2020). U.S. will reallocate military 3.5 GHz spectrum for CONSUMER 5G in 2021. VentureBeat. [Online]. https://venturebeat.com/2020/08/10/u-s-will-reallocate-military-3-5ghz-spectrum-for-consumer-5g-in-2021/

[4] J. L. Allen, "Gain and impedance variation in scanned dipole arrays," *IRE Trans. Antennas Propag.*, vol. 10, no. 5, pp. 566–572, Sep. 1962.

[5] J. Roessler et al., "Enhancing frequency-agile radar range over a broad operating bandwidth with reconfigurable transmitter amplifier matching networks," in *Proc. IEEE Radar Conf. (RadarConf)*, Atlanta, GA, USA, May 2021, pp. 1–5.

[6] R. M. Fano, "Theoretical limitations on the broadband matching of arbitrary impedances," *J. Franklin Inst.*, vol. 249, no. 2, pp. 139–154, Feb. 1950.

[7] H. W. Bode, *Network Analysis and Feedback Amplifier Design*. Princeton, NJ, USA: Van Nostrand, 1945.
[8] B. S. Yarman, "Modern approaches to broadband matching problems," *IEE Proc. H, Microw., Antennas Propag.*, vol. 132, no. 2, pp. 87–92, Apr. 1985.
[9] J.-S. Fu, X. A. Zhu, J. D. Phillips, and A. Mortazawi, "A ferroelectric-based impedance tuner for adaptive matching applications," in *IEEE MTT-S Int. Microw. Symp. Dig.*, Atlanta, GA, USA, Jun. 2008, pp. 955–958.
[10] J.-S. Fu, X. A. Zhu, J. D. Phillips, and A. Mortazawi, "Improving linearity of ferroelectric-based microwave tunable circuits," *IEEE Trans. Microw. Theory Techn.*, vol. 55, no. 2, pp. 354–360, Feb. 2007.
[11] A. Semnani, G. S. Shaffer, M. D. Sinanis, and D. Peroulis, "High-power impedance tuner utilising substrate-integrated evanescent-mode cavity technology and external linear actuators," *IET Microw., Antennas Propag.*, vol. 13, no. 12, pp. 2067–2072, Oct. 2019.
[12] *Maury Microwave*. Accessed: Jul. 2022. [Online]. Available: http://www.maurymw.com
[13] C. Sánchez-Pérez, C. M. Andersson, K. Buisman, D. Kuylenstierna, N. Rorsman, and C. Fager, "Design and large-signal characterization of high-power varactor-based impedance tuners," *IEEE Trans. Microw. Theory Techn.*, vol. 66, no. 4, pp. 1744–1753, Apr. 2018.
[14] Y. Lu, L. P. B. Katehi, and D. Peroulis, "High-power MEMS varactors and impedance tuners for millimeter-wave applications," *IEEE Trans. Microw. Theory Techn.*, vol. 53, no. 11, pp. 3672–3678, Nov. 2005.
[15] T. Singh, N. K. Khaira, and R. R. Mansour, "Monolithically integrated reconfigurable RF MEMS based impedance tuner on SOI substrate," in *IEEE MTT-S Int. Microw. Symp. Dig.*, Boston, MA, USA, Jun. 2019, pp. 790–792.
[16] D. Qiao, R. Molfino, S. M. Lardizabal, B. Pillans, P. M. Asbeck, and G. Jerinic, "An intelligently controlled RF power amplifier with a reconfigurable MEMS-varactor tuner," *IEEE Trans. Microw. Theory Techn.*, vol. 53, no. 3, pp. 1089–1095, Mar. 2005.
[17] A. van Bezooijen, M. A. de Jongh, F. van Straten, R. Mahmoudi, and A. H. M. van Roermund, "Adaptive impedance-matching techniques for controlling L networks," *IEEE Trans. Circuits Syst. I, Reg. Papers*, vol. 57, no. 2, pp. 495–505, Feb. 2010.
[18] Y. Sun, J. Moritz, and X. Zhu, "Adaptive impedance matching and antenna tuning for green software-defined and cognitive radio," in *Proc. IEEE 54th Int. Midwest Symp. Circuits Syst. (MWSCAS)*, Aug. 2011, pp. 1–4.
[19] A. Dockendorf et al., "Fast optimization algorithm for evanescent-mode cavity tuner optimization and timing reduction in software-defined radar implementation," *IEEE Trans. Aerosp. Electron. Syst.*, vol. 56, no. 4, pp. 2762–2778, Aug. 2020.
[20] A. Egbert, A. Goad, C. Baylis, A. Martone, B. Kirk, and R. Marks, II, "Continuous real-time circuit reconfiguration to maximize average output power in cognitive radar transmitters," *IEEE Trans. Aerosp. Electron. Syst.*, vol. 58, no. 3, pp. 1514–1527, Jun. 2022.
[21] C. Calabrese, A. Dockendorf, A. Egbert, B. Herrera, C. Baylis, and R. J. Marks, "Fast switched-stub impedance tuner reconfiguration for frequency and beam agile radar and electronic warfare applications," in *Proc. IEEE Int. Radar Conf. (RADAR)*, Bethesda, MD, USA, Apr. 2020, pp. 94–98.
[22] C. Calabrese et al., "A plasma-switch impedance tuner for real-time, frequency-agile, high-power radar transmitter reconfiguration," in *IEEE MTT-S Int. Microw. Symp. Dig.*, Atlanta, GA, USA, Jun. 2021, pp. 585–588.
[23] A. Fisher, Z. V. Missen, T. R. Jones, and D. Peroulis, "A fiber-free DC-7 GHz 35 W integrated semiconductor plasma switch," in *IEEE MTT-S Int. Microw. Symp. Dig.*, Atlanta, GA, USA, Jun. 2021, pp. 27–30.
[24] J. Roessler et al., "A low-loss reconfigurable plasma impedance tuner for real-time, frequency-agile, high-power RF applications," in *IEEE MTT-S Int. Microw. Symp. Dig.*, Denver, CO, USA, Jun. 2022, pp. 183–186.
[25] M. Vai and S. Prasad, "Automatic impedance matching with a neural network," *IEEE Microw. Guided Wave Lett.*, vol. 3, no. 10, pp. 353–354, Oct. 1993.
[26] M. Unlu et al., "A reconfigurable RF MEMS triple stub impedance matching network," in *Proc. Eur. Microw. Conf.*, Manchester, U.K., Sep. 2006, pp. 1370–1373.
[27] K. Saito et al., "Real-time impedance matching system using liquid stub tuners in ICRF heating," *Fusion Eng. Des.*, vol. 81, nos. 23–24, pp. 2837–2842, Nov. 2006.

Justin Roessler (Graduate Student Member, IEEE) received the B.S. degree in electrical and computer engineering from Baylor University, Waco, TX, USA, in 2020, where he is currently pursuing the M.S. and Ph.D. degrees in electrical and computer engineering under the supervision of Prof. Charles Baylis.

His research focuses on the development of high-power electrically actuated impedance tuners for real-time RF transmitter optimization.

Mr. Roessler received the Second Place in the Student Research Competition at the 2022 IEEE Texas Symposium on Wireless and Microwave Circuits and Systems.

Alden Fisher (Graduate Student Member, IEEE) received the B.S. degree in electrical engineering from Purdue University, West Lafayette, IN, USA, in 2017, where he is currently pursuing the Ph.D. degree under the supervision of Prof. Dimitrios Peroulis.

His current research interests include solid-state plasma devices and their role in reconfigurable, high-frequency, high-power electronics. He has also explored wireless energy transfer.

Mr. Fisher is a member of Eta Kappa Nu. He received the First Place in the Packaged C-Band Filter (MTT-5, MTT-16) Student Design Competition at IMS 2022. He was the Local MTT-S Chapter Chair.

Austin Egbert (Member, IEEE) received the B.S. degree in electrical and computer engineering from Baylor University, Waco, TX, USA, in 2017, and the M.S. and Ph.D. degrees in electrical and computer engineering from Baylor University in 2021.

He is currently an Assistant Research Scientist with the Spectrum Management with Adaptive and Reconfigurable Technologies (SMART) Hub, Baylor University, developing deployable solutions for modern spectrum issues involving real-time circuit optimization and dynamic spectrum allocation.

Zach Vander Missen received the B.S. and Ph.D. degrees in electrical engineering from Purdue University, West Lafayette, IN, USA, in 2016 and 2022, respectively.

He is currently a Senior Electrical Engineer at Skyworks Solutions, Inc., Irvine, CA, USA.

Dr. Vander Missen received the Best Student Paper Award at the IEEE WAMICON 2021 Conference. He was a recipient of the IEEE MTT-S IMS Graduate Student Challenge Award in 2018.

Trevor Van Hoosier (Graduate Student Member, IEEE) received the B.S. degree in electrical and computer engineering from Baylor University, Waco, TX, USA, in 2021, where he is currently pursuing the M.S. and Ph.D. degrees in electrical and computer engineering.

His research interests include spectral coexistence techniques and real-time circuit optimization for application to radar transmit amplifiers and fifth-generation (5G) systems.

Charles Baylis (Senior Member, IEEE) is currently a Professor of electrical and computer engineering at Baylor University, Waco, TX, USA. At Baylor University, he directs the Wireless and Microwave Circuits and Systems Program, launched in 2008 to provide wireless and microwave education and research in a caring, Christian environment. He is involved in research that applies this approach to wireless communications, radar, and passive sensing systems and their circuit and array technologies. His research has been funded by the Army Research Laboratory, the National Science Foundation, the Office of Naval Research, and the Naval Research Laboratory. His research interests include adaptive and reconfigurable circuits, systems, and policy for more efficient use of the wireless spectrum.

Mohammad Abu Khater (Senior Member, IEEE) received the Ph.D. degree in electrical and computer engineering from Purdue University, West Lafayette, IN, USA, in 2015.

He is currently a Research Scientist with Purdue University. He was with Qualcomm and Intel Labs, where he worked on various high-speed and low-power circuits and systems. His research interests are primarily focused on adaptive wireless devices, interference detection and suppression, and system-level RF designs.

Dr. Abu Khater was a recipient of the Best Paper Award (WAMICON 2022) and a co-recipient of the Best Paper Award from the IEEE MICROWAVE AND WIRELESS COMPONENT LETTERS. He received the Excellence in Teaching Award from the College of Engineering, Purdue University, in 2012. He received the Fulbright Graduate Scholarship.

Dimitrios Peroulis (Fellow, IEEE) received the Ph.D. degree in electrical engineering from the University of Michigan at Ann Arbor, Ann Arbor, MI, USA, in 2003.

He is currently the Reilly Professor and Michael and Katherine Birck Head of the Elmore Family School of Electrical and Computer Engineering, Purdue University, West Lafayette, IN, USA. He also serves as a special adviser to the Dean of Engineering on online learning. His research interests are focused on the areas of reconfigurable systems, cold-plasma RF electronics, and wireless sensors. He has been a key contributor in developing high-quality widely tunable filters and novel filter architectures based on miniaturized high-Q cavity-based resonators in the 1–100-GHz range. He is currently leading research efforts in high-power multifunctional RF electronics based on cold-plasma technologies. He has coauthored over 450 journal articles and conference papers.

Dr. Peroulis received the National Science Foundation CAREER Award in 2008. He received the "Tatsuo Itoh" Award in 2019 and the Outstanding Young Engineer Award in 2014 from the IEEE Microwave Theory and Techniques Society (MTT-S). In 2012, he received the Outstanding Paper Award from the IEEE Ultrasonics, Ferroelectrics, and Frequency Control Society (Ferroelectrics Section). His students have received numerous student paper awards and other student research-based scholarships. He has been a Purdue University Faculty Scholar and has also received 11 teaching awards, including the 2010 HKN C. Holmes MacDonald Outstanding Teaching Award and the 2010 Charles B. Murphy award, which is Purdue University's highest undergraduate teaching honor.

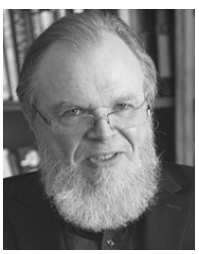

Robert J. Marks, II (Life Fellow, IEEE) received the Ph.D. degree from Texas Tech University, Lubbock, TX, USA, in 1977.

He is currently a Distinguished Professor of Engineering with the Department of Engineering and Computer Science, Baylor University, Waco, TX, USA, and the Director and a Senior Fellow of the Walter Bradley Center for Natural and Artificial Intelligence, Seattle, WA, USA. He has consulted for Microsoft, DARPA, and Boeing. He is the author or coauthor of *Neural Smithing: Supervised Learning in Feedforward Artificial Neural Networks* (MIT Press), *Handbook of Fourier Analysis and Its Applications* (Oxford University Press), *Introduction to Shannon Sampling and Interpolation Theory* (Springer-Verlag), and *Introduction to Evolutionary Informatics* (World Scientific).

Dr. Marks, II, is a Fellow of the Optical Society of America. He is the Editor-in-Chief of *BIO-Complexity* and the former Editor-in-Chief of the IEEE TRANSACTIONS ON NEURAL NETWORKS AND LEARNING SYSTEMS. His professional awards include the NASA Tech Brief Award and the IJCNN Pioneer in Neural Network Award. He is the Faculty Advisor for the Ratio Christi and American Scientific Affiliation Student Chapters at Baylor University.